Modulating Photo- and Radioluminescence in Tb(III) Cluster-Based Metal–Organic Frameworks

Zvart Ajoyan,†[ab] Gabrielle A. Mandl,†[ab] P. Rafael Donnarumma,[ab] Victor Quezada-Novoa,[ab] Hudson A. Bicalho,[ab] Hatem M. Titi,[bc] John A. Capobianco*[ab] and Ashlee J. Howarth*[ab]

[a] Department of Chemistry and Biochemistry and Centre for NanoScience Research, Concordia University, 7141 Sherbrooke Street West, Montréal, Quebec H4B 1R6, Canada
[b] FRQNT Quebec Centre for Advanced Materials (QCAM/CQMF), Montreal, Canada
[c] Department of Chemistry, McGill University, 801 Sherbrooke St. W., Montreal, Quebec H3A 0B8, Canada

Metal–Organic Frameworks, Photoluminescence, Radioluminescence, Lanthanide

Supporting Information Placeholder

ABSTRACT: Luminescent metal–organic frameworks (MOFs) are of interest for sensing, theranostics, dosimetry, and other applications. The use of lanthanoids in MOF metal nodes allows for intrinsic metal-based luminescence. In this work, a facile route for modulating the photoluminescent and radioluminescent properties of Tb(III)-based MOFs is reported. By using Tb(III)-cluster nodes as X-ray attenuators, and organic linkers with varying excited state energies as sensitizers, MOFs with metal-based, linker-based, and metal+linker-based photo- and radioluminescence are reported.

Luminescent materials are of interest for sensing,[1] security,[2] bioimaging,[3] solid-state lighting,[4] and other applications. Radioluminescent (RL) materials, in particular, emit light upon excitation with ionizing radiation. Radioluminescence arising from X-ray excitation is of interest for applications in dosimetry,[5] theranostics,[6] and security.[7] RL materials can be categorized as inorganic or organic.[8] In pure inorganic materials, radioluminescence is a property of the host material, with high Z elements used to attenuate X-rays through the photoelectric effect to give luminescence. In contrast, radioluminescence of organic materials arises from individual molecules, and the low Z nature of these materials results in inherently low X-ray absorption efficiencies. Thus, inorganic RL materials tend to have higher light output, while organic RL materials have more opportunity for color tunability through functional group modulation.[9]

Metal–organic frameworks (MOFs) are porous, often crystalline, materials[10-13] that have the potential to bridge the properties of traditional inorganic and organic RL materials. The metal nodes in MOFs can either be ion[14, 15], chain,[16, 17] or cluster-based[18, 19] with varying nuclearity, geometry, and connectivity. By controlling the identity of the metal node and organic linker, MOFs with tuneable luminescent properties can be obtained.[20, 21] To date, the majority of reported RL MOFs utilize high-Z metal nodes for X-ray attenuation, and organic linkers as the emitting species. [5, 6, 22-25] More recently, lanthanoid-based MOFs comprised of metal ion nodes have been shown to demonstrate metal-based radioluminescence.[26,27]

Herein, we report the photoluminescent and radioluminescent properties of three lanthanoid cluster-based MOFs, Tb-

UiO-66 (Figure 1a)[28], Tb-CU-10 (Figure 1b),[29] and the novel Tb-CU-27 (Figure 1c), which demonstrate metal-based, linker-based, and metal+linker based radioluminescence, respectively. The presence of multinuclear cluster nodes in these MOFs allows for strong X-ray attenuation while the varying triplet state energies of the linkers result in drastically different photo- and radioluminescence spectra. A comparison of their photophysical properties is presented, including an evaluation of radiation hardness up to 200 Gy.
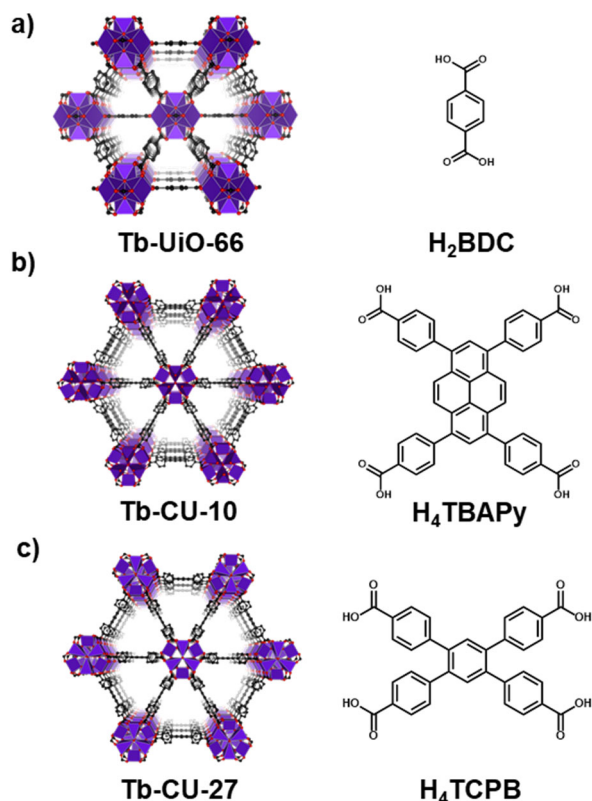

Figure 1. Structures and organic linker component of (a) Tb-UiO-66, (b) Tb-CU-10, and (c) Tb-CU-27.
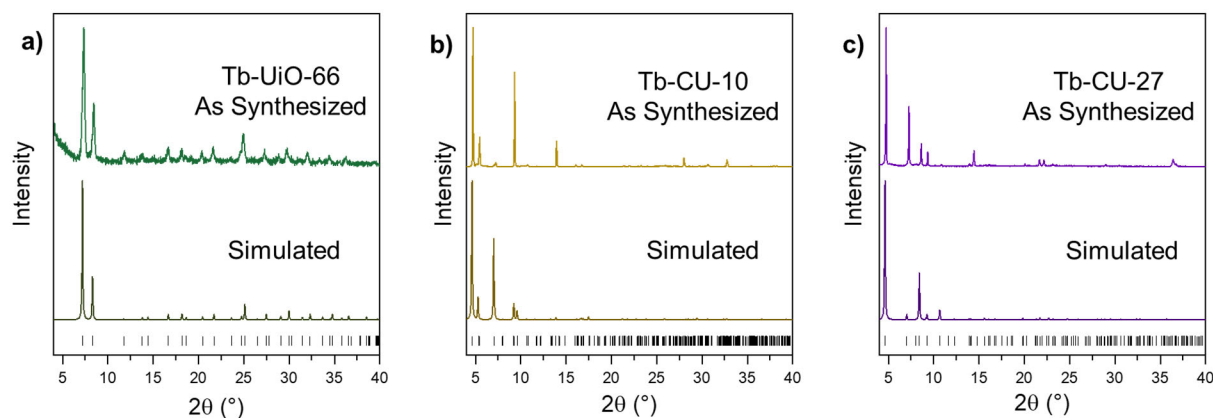
Figure 1. Powder X-ray diffractograms of (a) Tb-UiO-66, (b) Tb-CU-10 and (c) Tb-CU-27.

Three Tb(III)-MOFs were chosen for the present study owing to the variation in triplet excited state energy (T_1) of the structural organic linker. Tb-UiO-66, Tb-CU-10, and Tb-CU-27 are formed using 1,4-benzenedicarboxylic acid (H_2BDC), 1,3,6,8-tetrakis(p-benzoate)-pyrene (H_4TBAPy), and 1,2,4,5-tetrakis(4-carboxyphenyl)benzene (H_4TCPB), which have T_1 energies of 25 641,[30, 31] 16 938,[32] and 21 589 cm^{-1},[33] respectively (Figure S1). Given that these linker energies are higher, lower, and resonant with the $^5D_4$ state of Tb(III) (20 490 cm^{-1}), in conjunction with the high density of Tb(III) ions in the metal cluster nodes, we anticipated a range of photoluminescent and radioluminescent properties across the series. Tb-UiO-66 and Tb-CU-10 have been previously reported by our group,[28, 29] and Tb-CU-27 is a novel MOF that is a structural analogue of Y-**shp**-MOF-5.[34] Tb-UiO-66 is a lanthanoid analogue of the archetypical Zr-UiO-66, which is comprised of hexanuclear clusters bridged by ditopic linkers to give the **fcu** topology (Figure 1a). Tb-CU-10 and Tb-CU-27 are isoreticular and comprised of Tb$_9$-cluster nodes bridged by tetratopic linkers giving rise to the **shp** topology (Figure 1b,c).

Tb-UiO-66, Tb-CU-10, and Tb-CU-27 are synthesized under solvothermal conditions using Tb(NO$_3$)$_3$·xH$_2$O, a fluorinated modulator, and the respective organic linker. The phase purity of each MOF is confirmed by powder X-ray diffraction (PXRD) using simulated patterns as a comparison (Figure 2, Figure S2). Single-crystal X-ray diffraction (SCXRD) of the novel Tb-CU-27 shows a disordered nonanuclear metal cluster node that is 12-connected (Figure S3), and an overall **shp** topology (Figure S4, S5), similar to that observed in Y-**shp**-MOF-5,[34] and Tb-CU-10.[29] SCXRD of Tb-UiO-66 reveals the expected 12-connected hexanuclear metal cluster node and **fcu** topology (Figure S6). Scanning electron microscopy (SEM) micrographs of Tb-CU-27 and Tb-CU-10 show hexagonal-shaped crystallites of 120 μm and 240 μm, respectively (Figure S7a,b) and Tb-UiO-66 show octahedral crystallites of 25 μm (Figure S7c). Nitrogen sorption studies of Tb-UiO-66, Tb-CU-10, and Tb-CU-27, show reversible Type-I isotherms (Figure S8) with calculated BET surface areas and pore diameters of 840 m^2/g and 10 Å, 1665 m^2/g and 11 Å, and 1365 m^2/g and 11 Å, respectively. Diffuse reflectance infrared Fourier transform spectroscopy (DRIFTS) (Figure S9), ^{1}H-NMR spectroscopy (Figure S10), and thermogravimetric analysis (TGA) (Figure S11) of Tb-CU-27 are consistent with a formula of DMA[Tb$_9$(μ$_3$-X)$_{12}$(μ$_3$-O)$_2$(TCPB)$_3$]·DMF where X = OH or F. We previously reported formulas of DMA$_2$[Tb$_6$(μ$_3$-OH)$_8$(BDC)$_6$] for Tb-UiO-66[28] and DMA$_3$[Tb$_9$(μ$_3$-OH)$_{12}$(μ$_3$-O)$_2$(TBAPy)$_3$(2-FBA)$_2$]·(DMF)(2-HFBA) for Tb-CU-10.[29] A recent study[35] suggested the possibility that the μ$_3$-OH groups in

RE cluster-based MOFs synthesized using fluorinated modulators may be μ$_3$-F, which is difficult to distinguish crystallographically. As such, we have included the corresponding single-crystal X-ray structures with μ$_3$-F and μ$_3$-OH in all cases (see SI for details).

The photoluminescence emission spectrum of Tb-UiO-66 upon 355 nm excitation exhibits characteristic emissions of Tb(III) corresponding to the $^5D_4 \rightarrow {}^7F_{3,4,5,6}$ transitions, respectively (Figure 3a). Although the BDC^{2-} linker and Tb(III) are both excited at 355 nm (Figure S12), Tb-UiO-66 exhibits no fluorescence or phosphorescence from the BDC^{2-} linker, owing to the energy of its triplet state (25 641 cm^{-1}) relative to the $^5D_4$ level of Tb(III) (20 490 cm^{-1}).[30, 31] Efficient intersystem crossing (ISC) and population of the T_1 state of BDC^{2-} is expected to be facilitated by the heavy atom effect, resulting in strong sensitization of Tb(III) emissions *via* the antenna effect in Tb-UiO-66. The decay time of the $^5D_4 \rightarrow {}^7F_5$ transition (545 nm) of Tb-UiO-66 upon 355 nm excitation is 1048.6 ± 6.93 μs (Figure S13), which is typical for Tb(III) 4f-4f transitions. [36-38]

The radioluminescence emission spectrum of Tb-UiO-66 under 50 kVp, 80 μA unfiltered X-ray excitation (Au target) also exhibits characteristic Tb(III) emissions and no linker emission. Of all three MOFs, the radioluminescence intensity of Tb-UiO-66 is the most intense (Figure 3d, Figure S14), indicative of high X-ray attenuation by the hexanuclear Tb(III)-clusters coupled with the highly efficient sensitization of Tb(III) from the triplet state of BDC^{2-}. The density and Z_{eff} of the material (Figure S15, Table S1),[39] and lack of metal-to-ligand energy transfer (ET) facilitate strong X-ray attenuation and strong Tb(III)-based radioluminescence. As a control, all MOF starting materials were mixed in ratios similar to those found in each MOF, and no radioluminescence was observed, confirming that the multinuclear cluster node and overall network structure are required for efficient radioluminescence emission to occur (Figure S16).

Tb-CU-10 exhibits a broad, featureless emission band at 525 nm upon excitation at 355 nm (into the $S_0 \rightarrow S_n$ bands of TBAPy^{4-}, Figure S12) and upon X-ray excitation (Figure 3b). This broad emission band is characteristic of pyrene-based emission, with no features of Tb(III) emission observed. The
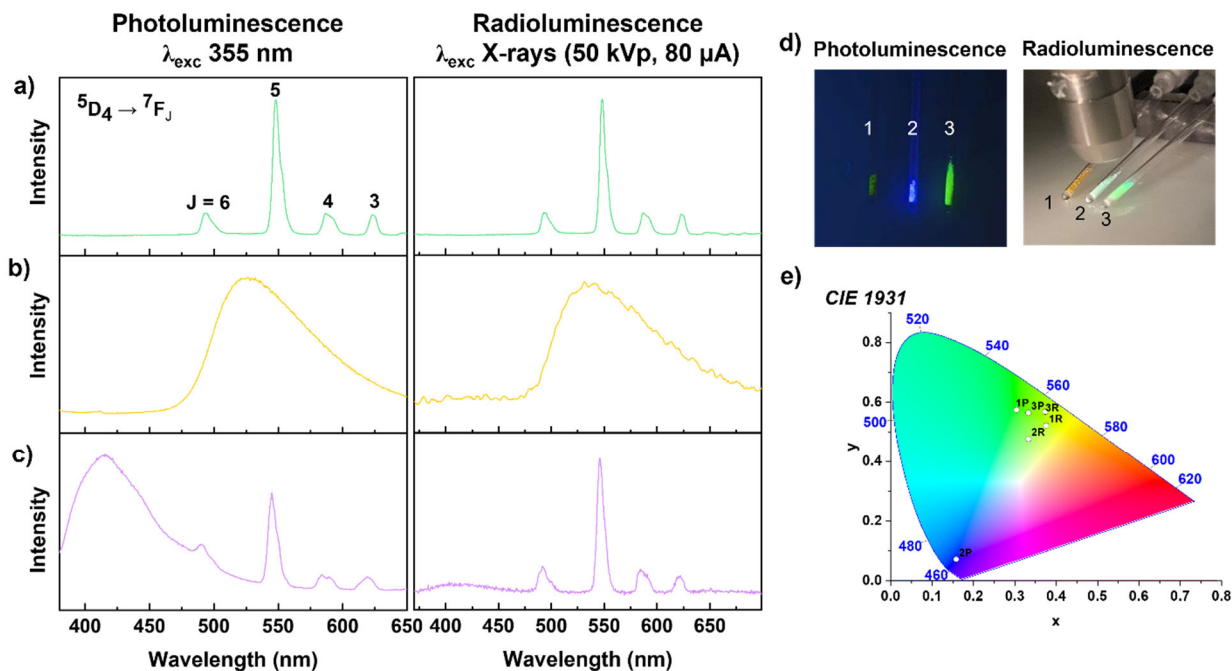
Figure 2. Photoluminescence (left) and radioluminescence (right) emission spectrum of (a) Tb-UiO-66, (b) Tb-CU-10, and (c) Tb-CU-27. Photographs of (1) Tb-CU-10, (2) Tb-CU-27 and (3) Tb-UiO-66 under UV (left) and X-ray (right) excitation. (e) CIE diagram of the photoluminescence (P) and radioluminescence (R) coordinates for each MOF.

triplet state of TBAPy[4-] is significantly lower energy than the $^5D_4$ level of Tb(III), near 16 938 cm^{-1}.[32] It has been previously demonstrated that the use of ligands with low energy triplet states in Tb(III) coordination compounds leads to quenching of Tb(III) luminescence.[40-43] Thus, the lack of Tb(III) emission in Tb-CU-10 is attributed to quenching from the pyrene linker.

The observed photo- and radioluminescence emission of Tb-CU-10, centered at 525 nm, is strongly red-shifted compared to the free linker (420 nm),[44] a commonly observed feature of excimer emission in pyrene-based MOFs.[45-47] Previous studies demonstrate that excimer formation in MOFs is favorable when the center-center distance between pyrene units is in the range of 8.8 – 11 Å, and the measured distance in Tb-CU-10 is 11 Å, in agreement with previous findings.[46] Furthermore, the pyrene-pyrene and pyrene-phenyl torsional angles are known to play a role in excimer formation,[46] where Tb-CU-10 exhibits torsional angles of 60 and 59° for pyrene-pyrene and pyrene-phenyl, respectively. These angles are similar to NU-1000 (60 and 50°), which is known to exhibit excimer emission.[46]

The weak linker-centered singlet excimer emission from Tb-CU-10 suggests efficient ISC and population of the linker triplet state may occur in the presence of Tb(III). This is corroborated by previously observed singlet oxygen production in this MOF, which is reliant on the population of the triplet state of the linker.[29] To further prove the role of the heavy atom effect on quenching the singlet excimer emission of the MOF, we synthesized Y-CU-10 and observed radioluminescence emission in the same position, but of significantly greater intensity (Figure S17). Since Y(III) is not considered a heavy atom compared to Tb(III), the rates of ISC are expected to be significantly reduced and thus singlet-state excimer emission becomes more favorable, resulting in the observed higher intensity.

The emission spectrum of Tb-CU-27 upon 355 nm excitation exhibits emission from both the TCPB[4-] linker and Tb(III) (Figure 3c). Owing to the strong absorption bands of TCPB[4-]

and Tb(III) at 355 nm (Figure S12), and the potential for sensitization between TCPB[4-] and Tb(III), photoluminescence is observed from both metal and linker components. As observed with Tb-UiO-66, the population of the T_1 state of the linker leads to $T_1 \rightarrow$ Tb(III) ET and Tb(III) emission. The strong emission at 420 nm is attributed to the $S_1 \rightarrow S_0$ emission of TCPB[4-] (28 169 cm^{-1}),[33] which suggests inefficient ISC to the T_1 state, favoring radiative recombination[48] and indicating that the $S_1 \rightarrow T_1 \rightarrow$ Tb(III) ET pathway may not be the most prominent route. Interestingly, the lifetime of the $^5D_4 \rightarrow {}^7F_5$ transition of Tb(III) upon 355 nm excitation was found to be 53.1 ± 0.08 μs (Figure S13), which is relatively short for this transition.[36-38] Since the emission of TCPB[4-] overlaps with the $^5D_4 \rightarrow {}^7F_5$ transition at 545 nm, and has a short decay time (on the order of ps-ns), the lifetime of the $^5D_4 \rightarrow {}^7F_3$ transition of Tb(III) at 621 nm was also measured. The decay time of this transition was found to be 51.6 ± 1.13 μs, which is similar to the $^5D_4 \rightarrow {}^7F_5$ transition, and is still unexpectedly short for a Tb(III) decay time (Figure S13). A decreased decay time is associated with the introduction of a de-excitation pathway of the $^5D_4$ state, which can be understood when one considers that the triplet state of TCPB[4-] is known to reside at 21 589 cm^{-1},[33] resonant with the $^5D_4$ level of Tb(III), resulting in efficient back ET from Tb(III) to TCPB[4-]. Back ET from the $^5D_4$ state of Tb(III) is known to occur when the ligand triplet state energy is below 22 300 cm^{-1}, as is the case here.[49]

The radioluminescence and photoluminescence emission spectra of Tb-CU-27 are markedly different (Figure 3c). Upon X-ray excitation, the linker emission is less intense than the emission from Tb(III), which is in contrast to what is observed upon UV excitation. The different emission properties can also be visually observed (Figure 3d,e), where the MOF exhibits predominately blue photo- and green radioluminescence. This can be explained by considering the efficiency of X-ray attenuation of the Tb(III) clusters vs. the linkers. Low-energy X-ray photons are efficiently attenuated by high-density, high-Z_{eff} materials, thus the structure of a cluster-based MOF has regions of high
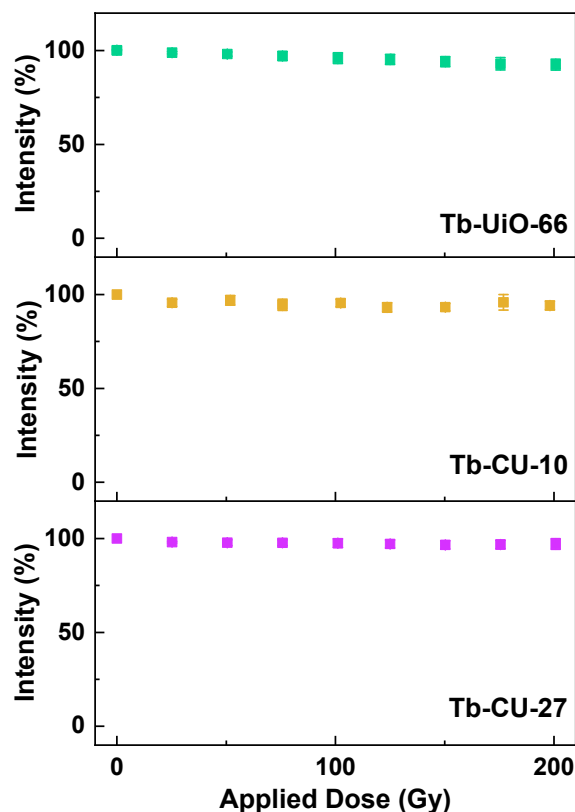
Figure 4. Radioluminescence intensity vs. applied X-ray dose of (a) Tb-UiO-66, (b) Tb-CU-10 and (c) Tb-CU-27.

(Tb(III) metal clusters) and low density/low Z_{eff} (pores and linkers), and it can be inferred that the majority of the incoming radiation is attenuated by the Tb(III) clusters. This is evidenced by strong Tb(III) radioluminescence and suggests the weak linker-based radioluminescence is due to secondary excitation. This postulation was confirmed by evaluating the radioluminescence spectrum of free TCPB^{4-} (Figure S18) where no radioluminescence was observed.

In order to assess the structural integrity of each MOF after extended doses of X-ray irradiation, radiation hardness measurements were performed on activated MOFs. Doses up to 200 Gy were delivered to the MOFs to evaluate their stability (Figure 4). Tb-UiO-66 was found to be radioresistant, exhibiting a 10 % loss of its radioluminescence intensity after exposure up to 200 Gy at a dose rate of 30 Gy/min (Figure 4a). The bulk crystallinity of Tb-UiO-66 remains intact (Figure S19a), although the BET surface area (Figure S20a) was found to decrease by approximately 24 % (from 840 to 640 m²/g), which is consistent with previous observations related to the gradual collapse of this MOF after activation.[28] Tb-CU-10 and Tb-CU-27 were found to be highly radioresistant with minimal changes in radioluminescence intensity as a function of applied dose (Figure 4b,c). The bulk crystallinity of Tb-CU-10 and Tb-CU-27 remains intact after exposure to X-ray doses of 200 Gy (Figure S19b,c), and the BET surface areas only decreased by 5 % (from 1630 to 1540 m²/g, Figure S20b) and 9% (995 to 900 m²/g , Figure S20c), respectively.

In summary, three luminescent Tb(III)-cluster-based MOFs are reported, where the photoluminescent and radioluminescent behaviour arises from a combination of the multinuclear cluster nodes and judiciously chosen organic linkers. Each MOF demonstrates a different emission profile which is attributed

to the differences in energies of the T_1 state of the organic linkers. Tb-UiO-66 possesses strong Tb(III)-centered photo- and radioluminescence, Tb-CU-10 demonstrates weak excimer linker-based photo- and radioluminescence, and Tb-CU-27 shows linker and metal-based photo- and radioluminescence. In addition, all three MOFs remain stable upon X-ray irradiation with doses up to 200 Gy. This study highlights the utility of cluster-based MOFs in attenuating X-rays to produce radioluminescent materials, and the importance of the role of linker triplet state energies in modulating the photo- and radioluminescence properties of Tb(III)-based MOFs.

ASSOCIATED CONTENT

Supporting Information

Details of synthesis, characterization, and additional data figures. (PDF)

The Supporting Information is available free of charge on the ACS Publications website.

AUTHOR INFORMATION

Corresponding Author

Department of Chemistry and Biochemistry, and Centre for NanoScience Research, Concordia University, 7141 Sherbrooke St W., Montréal, QC, Canada.
Email: john.capobianco@concordia.ca
Email: ashlee.howarth@concordia.ca

Author Contributions

†Z.A. and G. A. M. contributed equally. All authors have given approval to the final version of the manuscript.

Notes

The authors declare no competing financial interests

REFERENCES

1.   Zhang, Y.; Yuan, S.; Day, G.; Wang, X.; Yang, X.; Zhou, H.-C., Luminescent sensors based on metal-organic frameworks. *Coord. Chem. Rev.* **2018,** *354*, 28-45.
2.   Liu, J.; Zhuang, Y.; Wang, L.; Zhou, T.; Hirosaki, N.; Xie, R.-J., Achieving Multicolor Long-Lived Luminescence in Dye-Encapsulated Metal–Organic Frameworks and Its Application to Anticounterfeiting Stamps. *ACS Appl. Mater. Interfaces* **2018,** *10* (2), 1802-1809.
3.   Demir Duman, F.; Forgan, R. S., Applications of nanoscale metal–organic frameworks as imaging agents in biology and medicine. *J Mater Chem B* **2021,** *9* (16), 3423-3449.

4.   Chen, D.-H.; Sedykh, A. E.; Gomez, G. E.; Neumeier, B. L.; Santos, J. C. C.; Gvilava, V.; Maile, R.; Feldmann, C.; WÖll, C.; Janiak, C.; Müller-Buschbaum, K.; Redel, E., SURMOF Devices Based on Heteroepitaxial Architectures with White-Light Emission and Luminescent Thermal-Dependent Performance. *Adv. Mater. Interfaces* **2020,** *7* (24), 2000929.

5.   Liu, H.; Qin, H.; Shen, N.; Yan, S.; Wang, Y.; Yin, X.; Chen, X.; Zhang, C.; Dai, X.; Zhou, R.; Ouyang, X.; Chai, Z.; Wang, S., Emergence of a Radical-Stabilizing Metal–Organic Framework as a Radio-photoluminescence Dosimeter. *Angew. Chem. Int. Ed.* **2020,** *59* (35), 15209-15214.

6.   Neufeld, M. J.; Lutzke, A.; Pratx, G.; Sun, C., High-Z Metal-Organic Frameworks for X-ray Radiation-Based Cancer Theranostics. *Chemistry* **2021,** *27* (10), 3229-3237.

7.   Wang, Y.; Liu, X.; Li, X.; Zhai, F.; Yan, S.; Liu, N.; Chai, Z.; Xu, Y.; Ouyang, X.; Wang, S., Direct Radiation Detection by a Semiconductive Metal–Organic Framework. *J. Am. Chem. Soc.* **2019,** *141* (20), 8030-8034.

8.   Klein, J. S.; Sun, C.; Pratx, G., Radioluminescence in biomedicine: physics, applications, and models. *Phys. Med. Biol.* **2019,** *64* (4), 04TR01.

9.   Maddalena, F.; Tjhajana, L.; Xie, A.; Arramel; Zeng, S.; Wang, H.; Coquet, P.; Drozdowski, W.; Dujardin, C.; Dang, C.; Birowosuto, M. D., Inorganic, Organic, and Perovskite Halides with Nanotechnology for High–Light Yield X- and γ-ray Scintillators. *Crystals* **2019,** *9* (2).

10.   Hoskins, B. F.; Robson, R., Design and construction of a new class of scaffolding-like materials comprising infinite polymeric frameworks of 3D-linked molecular rods. A reappraisal of the zinc cyanide and cadmium cyanide structures and the synthesis and structure of the diamond-related frameworks [N(CH3)4][CuIZnII(CN)4] and CuI[4,4',4'',4'''-tetracyanotetraphenylmethane]BF4.xC6H5NO2. *J. Am. Chem. Soc.* **1990,** *112* (4), 1546-1554.

11.   Kondo, M.; Yoshitomi, T.; Matsuzaka, H.; Kitagawa, S.; Seki, K., Three-Dimensional Framework with Channeling Cavities for Small Molecules: {[M2(4, 4′-bpy)3(NO3)4]·xH2O}n (M   Co, Ni, Zn). *Angew. Chem. Int. Ed.* **1997,** *36* (16), 1725-1727.

12.   Li, H.; Eddaoudi, M.; O'Keeffe, M.; Yaghi, O. M., Design and synthesis of an exceptionally stable and highly porous metal-organic framework. *Nature* **1999,** *402* (6759), 276-279.

13.   Furukawa, H.; Cordova, K. E.; O'Keeffe, M.; Yaghi, O. M., The Chemistry and Applications of Metal-Organic Frameworks. *Science* **2013,** *341* (6149), 1230444.

14.   He, Y.; Furukawa, H.; Wu, C.; O'Keeffe, M.; Chen, B., A mesoporous lanthanide–organic framework constructed from a dendritic hexacarboxylate with cages of 2.4 nm. *CrystEngComm* **2013,** *15* (45), 9328-9331.

15.   de Lill, D. T.; Cahill, C. L., An unusually high thermal stability within a novel lanthanide 1,3,5-cyclohexanetricarboxylate framework: synthesis, structure, and thermal data. *Chem. Commun.* **2006,** (47), 4946-4948.

16.   Serpaggi, F.; Férey, G., Hybrid open frameworks (MIL-n). Part 4 Synthesis and crystal structure of MIL-8, a series of lanthanide glutarates with an open framework, [Ln(H2O)]2[O2C(CH2)3CO2]3·4H2O. *J. Mater. Chem.* **1998,** *8* (12), 2737-2741.

17.   Kiritsis, V.; Michaelides, A.; Skoulika, S.; Golhen, S.; Ouahab, L., Assembly of a Porous Three-Dimensional Coordination Polymer: Crystal Structure of {[La2(adipate)3(H2O)4]6H2O}n. *Inorg. Chem.* **1998,** *37* (13), 3407-3410.

18.   Wang, Y.; Feng, L.; Fan, W.; Wang, K.-Y.; Wang, X.; Wang, X.; Zhang, K.; Zhang, X.; Dai, F.; Sun, D.; Zhou, H.-C., Topology Exploration in Highly Connected Rare-Earth Metal–Organic Frameworks via Continuous Hindrance Control. *J. Am. Chem. Soc.* **2019,** *141* (17), 6967-6975.

19.   Luebke, R.; Belmabkhout, Y.; Weseliński, Ł. J.; Cairns, A. J.; Alkordi, M.; Norton, G.; Wojtas, Ł.; Adil, K.; Eddaoudi, M., Versatile rare earth hexanuclear clusters for the design and synthesis of highly-connected ftw-MOFs. *Chem. Sci.* **2015,** *6* (7), 4095-4102.

20.   Cui, Y.; Yue, Y.; Qian, G.; Chen, B., Luminescent Functional Metal–Organic Frameworks. *Chem. Rev.* **2012,** *112* (2), 1126-1162.

21.   Allendorf, M. D.; Bauer, C. A.; Bhakta, R. K.; Houk, R. J. T., Luminescent metal–organic frameworks. *Chem. Soc. Rev.* **2009,** *38* (5), 1330-1352.

22.   Bauer, C. A.; Timofeeva, T. V.; Settersten, T. B.; Patterson, B. D.; Liu, V. H.; Simmons, B. A.; Allendorf, M. D., Influence of Connectivity and Porosity on Ligand-Based Luminescence in Zinc Metal–Organic Frameworks. *J. Am. Chem. Soc.* **2007,** *129* (22), 7136-7144.

23.   Mathis Ii, S. R.; Golafale, S. T.; Bacsa, J.; Steiner, A.; Ingram, C. W.; Doty, F. P.; Auden, E.; Hattar, K., Mesoporous stilbene-based lanthanide metal organic frameworks: synthesis, photoluminescence and radioluminescence characteristics. *Dalton Trans.* **2017,** *46* (2), 491-500.

24.   Wang, C.; Volotskova, O.; Lu, K.; Ahmad, M.; Sun, C.; Xing, L.; Lin, W., Synergistic Assembly of Heavy Metal Clusters and Luminescent Organic Bridging Ligands in Metal–Organic Frameworks for Highly Efficient X-ray Scintillation. *J. Am. Chem. Soc.* **2014,** *136* (17), 6171-6174.

25.   Perry Iv, J. J.; Feng, P. L.; Meek, S. T.; Leong, K.; Doty, F. P.; Allendorf, M. D., Connecting structure with function in metal–organic frameworks to design novel photo- and radioluminescent materials. *J. Mater. Chem.* **2012,** *22* (20), 10235-10248.

26.   Neufeld, M. J.; Winter, H.; Landry, M. R.; Goforth, A. M.; Khan, S.; Pratx, G.; Sun, C., Lanthanide Metal–Organic Frameworks for Multispectral Radioluminescent Imaging. *ACS Appl. Mater. Interfaces* **2020,** *12* (24), 26943-26954.

27.   Wang, X.; Wang, Y.; Wang, Y.; Liu, H.; Zhang, Y.; Liu, W.; Wang, X.; Wang, S., Color-tunable X-ray scintillation based on a series of isotypic lanthanide–organic frameworks. *Chem. Commun.* **2020,** *56* (2), 233-236.

28.   Donnarumma, P. R.; Frojmovic, S.; Marino, P.; Bicalho, H. A.; Titi, H. M.; Howarth, A. J., Synthetic approaches for accessing rare-earth analogues of UiO-66. *Chem. Commun.* **2021,** *57* (50), 6121-6124.

29.   Quezada-Novoa, V.; Titi, H. M.; Sarjeant, A. A.; Howarth, A. J., Building a shp: A Rare-Earth Metal–Organic Framework and Its Application in a Catalytic Photooxidation Reaction. *Chem. Mater.* **2021,** *33* (11), 4163-4169.

30.   Briones, D.; Leo, P.; Cepeda, J.; Orcajo, G.; Calleja, G.; Sanz, R.; Rodríguez-Diéguez, A.; Martínez, F., Alkaline-earth metal based MOFs with second scale long-lasting phosphor behavior. *CrystEngComm* **2018,** *20* (33), 4793-4803.

31.   Kuno, S.; Akeno, H.; Ohtani, H.; Yuasa, H., Visible room-temperature phosphorescence of pure organic crystals via a radical-ion-pair mechanism. *Phys. Chem. Chem. Phys.* **2015,** *17* (24), 15989-15995.

32.   Howarth, A. J. Bis-cyclometallated iridium(III) complexes bearing pyridineimine and salicylimine ancillary ligands : synthesis, characterization and applications. Thesis, 2014.

33.   Surbella III, R. G.; Carter, K. P.; Lohrey, T. D.; Reilly, D.; Kalaj, M.; McNamara, B. K.; Schwantes, J.; Abergel, R. J., Rational Design of a Uranyl Metal–Organic Framework for the Capture and Colorimetric Detection of Organic Dyes. *Chem. Eur. J.* **2020,** *26* (61), 13819-13825.

34.   AbdulHalim, R. G.; Bhatt, P. M.; Belmabkhout, Y.; Shkurenko, A.; Adil, K.; Barbour, L. J.; Eddaoudi, M., A Fine-Tuned Metal–Organic Framework for Autonomous Indoor Moisture Control. *J. Am. Chem. Soc.* **2017,** *139* (31), 10715-10722.

35.   Vizuet, J. P.; Mortensen, M. L.; Lewis, A. L.; Wunch, M. A.; Firouzi, H. R.; McCandless, G. T.; Balkus, K. J., Fluoro-Bridged Clusters in Rare-Earth Metal–Organic Frameworks. *J. Am. Chem. Soc.* **2021,** *143* (43), 17995-18000.

36.   Tessitore, G.; Maurizio, S. L.; Sabri, T.; Capobianco, J. A., Intrinsic Time-Tunable Emissions in Core–Shell Upconverting Nanoparticle Systems. *Angew. Chem. Int. Ed.* **2019,** *58* (29), 9742-9751.

37.   Parra, D. F.; Mucciolo, A.; Brito, H. F., Green luminescence system containing a Tb3+-β-diketonate complex doped in the epoxy resin as sensitizer. *J. Appl. Polym. Sci.* **2004,** *94* (3), 865-870.

38.   Ananias, D.; Firmino, A. D. G.; Mendes, R. F.; Paz, F. A. A.; Nolasco, M.; Carlos, L. D.; Rocha, J., Excimer Formation in a Terbium Metal–Organic Framework Assists Luminescence Thermometry. *Chem. Mater.* **2017,** *29* (21), 9547-9554.

39.   Taylor, M. L.; Smith, R. L.; Dossing, F.; Franich, R. D., Robust calculation of effective atomic numbers: The Auto-Zeff software. *Med Phys* **2012,** *39* (4), 1769-1778.

40.   Kleinerman, M., Energy Migration in Lanthanide Chelates. *J. Chem. Phys.* **1969,** *51* (6), 2370-2381.

41.   Santos, B. S.; de Mello Donegá, C.; de Sá, G. F., Photophysical properties of Eu3+, Gd3+ and Tb3+ complexes with 2-hydroxy-2,4,6-cycloheptatrien-1-one. *J. Lumin.* **1997,** *72-74*, 535-537.

42.   Santos, B. S.; de Mello Donegá, C.; de Sá, G. F.; de Oliveira, L. F. C.; Santos, P. S., Spectroscopy and non-radiative processes in Gd3+, Eu3+ and Tb3+ tropolonates. *Spectrochim. Acta A Mol. Biomol. Spectrosc.* **1998,** *54* (13), 2237-2245.

43.   de Sá, G. F.; Malta, O. L.; de Mello Donegá, C.; Simas, A. M.; Longo, R. L.; Santa-Cruz, P. A.; da Silva, E. F., Spectroscopic properties and design of highly luminescent lanthanide coordination complexes. *Coord. Chem. Rev.* **2000,** *196* (1), 165-195.

44.   Caballero-Mancebo, E.; Cohen, B.; Smolders, S.; De Vos, D. E.; Douhal, A., Unravelling Why and to What Extent the Topology of Similar Ce-Based MOFs Conditions their Photodynamic: Relevance to Photocatalysis and Photonics. *Adv. Sci.* **2019,** *6* (19), 1901020.

45.   Gutierrez, M.; Cohen, B.; Sánchez, F.; Douhal, A., Photochemistry of Zr-based MOFs: ligand-to-cluster charge transfer, energy transfer and excimer formation, what else is there? *Phys. Chem. Chem. Phys.* **2016,** *18* (40), 27761-27774.

46.   Deria, P.; Yu, J.; Smith, T.; Balaraman, R. P., Ground-State versus Excited-State Interchromophoric Interaction: Topology Dependent Excimer Contribution in Metal–Organic Framework Photophysics. *J. Am. Chem. Soc.* **2017,** *139* (16), 5973-5983.

47.   Kinik, F. P.; Ortega-Guerrero, A.; Ongari, D.; Ireland, C. P.; Smit, B., Pyrene-based metal organic frameworks: from synthesis to applications. *Chem. Soc. Rev.* **2021,** *50* (5), 3143-3177.

48.   Vila-Nova, S. P.; Pereira, G. A. L.; Albuquerque, R. Q.; Mathis, G.; Bazin, H.; Autiero, H.; Sá, G. F. d.; Alves, S., Study of the luminescence of Eu(III), Tb(III) and Gd(III) cryptates containing Py(CO2Et)2 as ligands. *J. Lumin.* **2004,** *109* (3), 173-179.

49.   Latva, M.; Takalo, H.; Mukkala, V.-M.; Matachescu, C.; Rodríguez-Ubis, J. C.; Kankare, J., Correlation between the lowest triplet state energy level of the ligand and lanthanide(III) luminescence quantum yield. *J. Lumin.* **1997,** *75* (2), 149-169.

50.   Momma, K.; Izumi, F., VESTA 3 for three-dimensional visualization of crystal, volumetric and morphology data. *J. Appl. Crystallogr.* **2011,** *44* (6), 1272-1276.

FOR TABLE OF CONTENTS ONLY

Tb-UiO-66

Tb-CU-27

Tb-CU-10

UV light
355 nm

X-rays
50 kVp (Au)